Convergence study of the Immersed Domain method for periodic particle configurations

Raphael Schubert*, Torsten Kraft, Claas Bierwisch

Fraunhofer IWM, Wöhlerstraße 11, 79108 Freiburg, Germany

{*raphael.schubert, torsten.kraft, claas.bierwisch*}*@iwm.fraunhofer.de*

Abstract

For large-scale discrete element (DEM) simulations, particles sizes are often scaled up to reduce the computational effort. This coarse graining is incompatible with certain types of coupling to computational fluid dynamics (CFD) simulations usually used for large-scale simulations, as they require the fluid cells to be even larger than the particles, leading to unacceptably badly resolved flows. We investigate the possibility of using an immersed domain method with a large cell size to perform coupled DEM-CFD simulations of dense granular flows. To this end, we calculate the drag force on a single particle of an infinite simple cubic array of spherical particles suspended in a driven flow. We consider three packing fractions and compare the results for multiple resolutions to those obtained from conformal mesh CFD. While a number of flow characteristics suffer badly from coarse resolutions, the total drag force on the particle proves surprisingly accurate even for resolutions lower than 10 cells per particle diameter.

Keywords: immersed domain, immersed boundary, particle drag force, computational fluid dynamics

*Corresponding author

1. Introduction

For powders used in industrial processes, interaction with the surrounding medium (gas/liquid) is often non-negligible. This poses an additional challenge to those wanting to simulate such processes on an realistic scale. In simulations at these scales, the powder particles are usually simulated using the Discrete Element Method (DEM) [1], for which there exist two different types of coupling to Computational Fluid Dynamics (CFD) solvers, referred to as either resolved or unresolved depending on the relative sizes of DEM particles and CFD cells [2]. In the case of resolved coupling, the spatial resolution of the fluid model is finer than the particle size which allows to simulate a detailed velocity and pressure field around each particle. In the case of unresolved coupling, the fluid resolution is coarser than the particle size which naturally prohibits such detailed modeling of the fields but renders faster computation of the CFD solution possible.

In most applications, treating the particles at their actual size would necessitate simulating a prohibitively large number of particles. Therefore, DEM particles are usually scaled by a factor larger than one, but in such a way that they still resolve the smallest geometric feature with sufficient accuracy (see e.g. [3] for details of this coarse graining technique).

Using such a coarse graining approach leads to a problem in the unresolved case—where the particles are smaller than the mesh cells used to solve the fluid equations—because the resolution of the flow becomes unacceptably coarse. Decreasing the particle scaling factor is often not an option, as the computational times of DEM simulations are usually orders of magnitude larger than those of CFD simulations and scale with the number of particles.

On the other hand, using resolved coupling requires a large number of fluid cells per particle, which quickly leads to the CFD simulations dominating the computational cost. Therefore, it is desirable to keep the size of the fluid cells as large a possible while still obtaining sufficiently accurate drag forces on the particles.

Different numerical schemes for the simulation of resolved flow exist. Maybe

the most obvious one uses a conformal mesh, where only the fluid domain is meshed and the volume occupied by the particles is left void. In a dynamic simulation where the particles move around, this requires constant remeshing, adding to the computational cost.

To avoid remeshing in dynamic CFD simulations with fluid-structure interactions, Peskin developed the Immersed Boundary (IB) method [4], originally to simulate arterial bivalves. The IB method avoids remeshing by solving the fluid equations on a static grid while enforcing the boundary conditions at the immersed boundary through the introduction of additional force terms in the Navier-Stokes equations. In n-dimensional space, the original method enables the embedding of $(n-1)$-dimensional structures: fibers in two dimensions or surfaces in three dimensions. Further development led to other methods variously called Immersed Domain (ID) method or Ficticous Domain method [5, 6] which are able to treat immersed n-dimensional bodies. For a review of IB and ID methods, we direct the reader to [7, 8].

The spatial convergence of IB methods depends, among other factors, on the concrete method and the problem. The IB method has been known to be formally second-order convergent [9, 10, 11], the actual convergence exponent depends on the smoothness of the problem and the discrete delta functions used in interpolation, though actual or close to seconder-order convergence has first been achieved by Griffith et al. [10] and later by Mori et al. [11] for an oscillating membrane in two dimensions. Tang et al. [12] find second order convergence for a periodic face-centered cubic (fcc) array of spheres. Blais et al. [13] report convergence of order 1.33 for Taylor-Couette flow.

The Cartesian Grid Method presented in [14] is shown to be second order accurate for Wannier flow in the Stokes regime. The Conservative Immersed Interface Method (CIIM) exhibits second order convergence for a variety of problems, which include flow in an inclined (relative to the grid) channel and around round and square cylinders [15, 16]. Depending on the problem, the convergence order of the ID method can range from one to two [6, 17]. Glowinski et al. [5] achieve resolution independence for the case of two sedimenting spheres

for resolutions above 64 fluid cells per diameter, while Hager et al. [18] claim eight cells per diameter to be sufficient for a single sphere. For the cases of an isolated sphere and cylinder simulated using CIIM, Pepiot et al. [16] report good results using 12.8 and acceptable results for just six cells per diameter.

As is evident already from the two particle case [5, 19], particles in fluids can strongly interact not only through direct contact but also through modified flow conditions. Hill et al. [20] and Beetstra et al. [21] use the Lattice Boltzmann method to solve flow through a simple cubic (sc) array of spheres to obtain drag relations, while Fattahi et al. [22] use it to evaluate various Lattice Boltzmann collision operators. Tang et al. [12] simulate the flow through an fcc array to obtain volumetric correction factors to compensate systematic errors of their IB method.

This leads to the scope of the present work. We propose steady flow through a simple cubic (sc) array of spheres as a model system to investigate the spatial convergence of the ID method in the presence of other particles. The problem is rather easy to handle computationally and possesses an approximate analytical solution for the Stokes limit [23]. This solution, however, is only of minor interest here. Foremost, because the technological applications of interest to the authors fall outside the Stokes regime and, furthermore, because the ID implementation used herein only works for moderate Reynolds numbers, although improvements have been reported [24]. We therefore focus on higher but moderate Reynolds numbers ($20 < \mathrm{Re} < 50$) and compare the ID results to those obtained from a Finite Volume method using a conformal mesh.

This article is organized as follows. First, the numerical methods are summarized and the simulation setups are explained in Section 2. Subsequently, the results are presented and discussed in Section 3. Finally, the study is concluded in Section 4.

2. Model description

2.1. Numerical schemes

The Immersed Domain simulation is carried out using *cfdemSolverIB* presented in [19], which implements the ID method to couple the open-source CFD package OpenFOAM [25] and the open-source DEM package LIGGGHTS [26].

Both *cfdemSolverIB* and the OpenFOAM solver *pisoFoam* we use for the conformal mesh simulations implement a Finite Volume scheme to solve the Navier-Stokes equations using the PISO (pressure-implicit split-operator) algorithm [27]. The important difference regarding our study is the treatment of particles suspended in the fluid.

For *pisoFoam*, a particle is simply a hole in the mesh with approriate boundary conditions applied to the newly formed internal boundary. We fully specify the boundary conditions we use in Section 2.4.

The ID solver *cfdemSolverIB*, on the other hand and despite its name, uses a variant of the Immersed Domain method to simulate particle-fluid interactions. It does so on the CFD side by treating the particles as another fluid phase, making it effectively a two-phase solver. Information about the particle phase is incorporated into the CFD solution by modifying the velocity field to be equal to the particle velocity at all locations inside that particle. After this modification, the velocity field has to be corrected to satisfy continuity.

The total drag force on a particle is obtained from the surface integral of the stress tensor σ over the particle's surface $\partial\Omega$, applying the divergence theorem and assuming a Newtonian fluid:

$$F = \int_{\partial\Omega} \sigma \, \mathrm{d}\mathbf{A} = \int_{\Omega} \operatorname{div} \sigma \, \mathrm{d}V = \int_{\Omega} \{-\nabla p + \nu\rho\Delta U\} \, \mathrm{d}V = F_p + F_{\nabla U}, \qquad (1)$$

where p is the pressure, U is the velocity, ν the kinematic viscosity and ρ the density of the fluid, which we set to $1\,\mathrm{kg/m^3}$. In the discrete case, the integral turns into a sum over all cells occupied by the particle. We discuss some consequences of this scheme in Section 3.2. For details, we refer the reader to [19].

We would like to draw attention to the decomposition of the total force into two contributions: a pressure term F_p and a viscous term $F_{\nabla U}$, which we later discuss in 3.3.1

2.2. Setup

We investigate the flow through an infinite simple cubic lattice of spheres at different packing densities ϕ. A single cubic unit cell is simulated using periodic boundary conditions in all directions. Packing densities are restricted to approximately $\phi = 22\,\%$, $6.5\,\%$ and $0.8\,\%$, corresponding to a particle of diameter $D = 1.5\,\mathrm{m}, 1\,\mathrm{m}$ and $0.5\,\mathrm{m}$, respectively, in a cubic domain with linear size $L = 2\,\mathrm{m}$.

2.3. Meshes

2.3.1. Immersed Domain

As commonly done in ID simulations, we use a regular hex mesh with constant cell size. We define the resolution of the simulation ρ to be the ratio between the particle diameter D and the linear cell size $c = L/N$:

$$\rho = \frac{D}{c}. \tag{2}$$

We vary ρ in the range from 2.5 to 47.5.

2.3.2. Conformal mesh

In order to generate accurate reference values to compare those obtained from the ID method to, we solve the same problem on a body-conforming mesh using a transient solver implementing the PISO scheme. The fluid domain (the unit cell excluding the volume occupied by the particle) is meshed using local refinement and including boundary layers along the sphere surface. We show a slice of the mesh in the top half of Fig. 1. The coarsest resolution corresponds to a regular hex mesh with $N = 40$. The total number of cells ranges from 370,000 for $D = 0.5\,\mathrm{m}$ to 2,500,000 for $D = 1.5\,\mathrm{m}$.

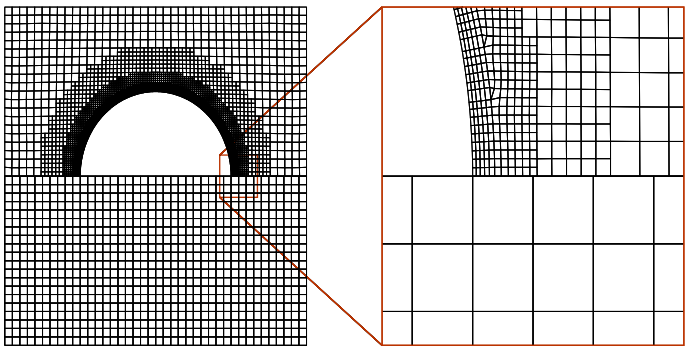

Figure 1: Comparison of the meshes used for conformal mesh (top half, $D = 1.0\,\mathrm{m}$) and ID simulations (bottom half, $N = 40$).

2.4. Boundary conditions

To simulate an infinite array of spheres, cyclic boundary conditions are specified on all external boundaries for all quantities with the exception of pressure. There, boundary conditions are also fundamentally cyclic, but in order to drive the flow, a jump Δp, which is constant in time and space, is imposed across the boundaries in x-direction.

In the conformal mesh simulation, we further specify no-slip boundary conditions on the sphere surface by specifying a value of zero for the velocity and zero gradient for pressure.

Fixing the kinematic viscosity at $\nu = 10^{-2}\ \mathrm{m}^2/\mathrm{s}$, we control the flow regime by adjusting Δp. The Reynolds number for this problem is defined as

$$\mathrm{Re} = \frac{U_s D}{\nu}, \tag{3}$$

where $U_s = (1 - \phi)\langle U \rangle$ is the superficial velocity and $\langle U \rangle$ denotes the spatial average of the velocity over the domain. Using this definition, our simulations are carried out at $\mathrm{Re} \approx 50, 40, 20$ for $D = 0.5\,\mathrm{m}, 1.0\,\mathrm{m}, 1.5\,\mathrm{m}$ respectively.

Using the largest flow velocity $U_{\max}$ instead of the superficial velocity U_s yields an alternative definition $\mathrm{Re}_{\max}$, with our simulations carried out at $\mathrm{Re}_{\max} \approx 64 - 69$ for all diameters.

2.4.1. Corrected pressure

With the specified boundary conditions, the pressure field assumes the form $p(\mathbf{x}) = p_0(\mathbf{x}) + \mathbf{I}(\mathbf{x}) \cdot \Delta\mathbf{p}$, where p_0 is the pressure field in the simulated reference domain, $\mathbf{I}(\mathbf{x})$ the image containing the point $\mathbf{x}$ and $\Delta\mathbf{p} = (\Delta p, 0, 0)$.

We can also regard p a superposition of a periodic and a linear component, $p = p_{\text{periodic}} + p_{\text{linear}}$, where $p_{\text{linear}}(x, y, z) = \Delta p \; x/L$. We will focus on the periodic component in the remainder of this article, so any unqualified mention of p and pressure will refer to the periodic component p_{periodic}.

2.5. Force reference values

In [28], Adler proposes a relation between the average pressure gradient in flow direction ∇P and the total drag force F_{D} exerted by the fluid:

$$\nabla P = -\frac{F_{\text{D}}}{L^3} \tag{4}$$

Since we prescribe the pressure gradient $\nabla P = \Delta p/L$, we can use this to calculate reference values for the drag force

$$F_{\text{ref}} := F_{\text{D}} = -\Delta p L^2 \tag{5}$$

which we will use as comparison for the simulated values in Section 3.3.

3. Results and discussion

3.1. Flow fields

The solutions for the velocity field (Fig. 2a and c) are qualitatively and quantitatively very similar for the two methods. Plotting U_x along a line connecting the sphere center at $(0, 0, 0)$ and the point directly between four spheres $(1, 0, 1)$, we find convergence of the curve towards the conformal solution (see Fig. 3). We notice, however, that the sphere is not completely impenetrable, evidenced by the finite value of the velocity field for $d < \frac{D}{2}$. This behaviour is consistent with the observation from the pressure images in Fig. 2b and d, that for ID, the pressure in the stagnation zone is lower than for the conformal mesh case. The

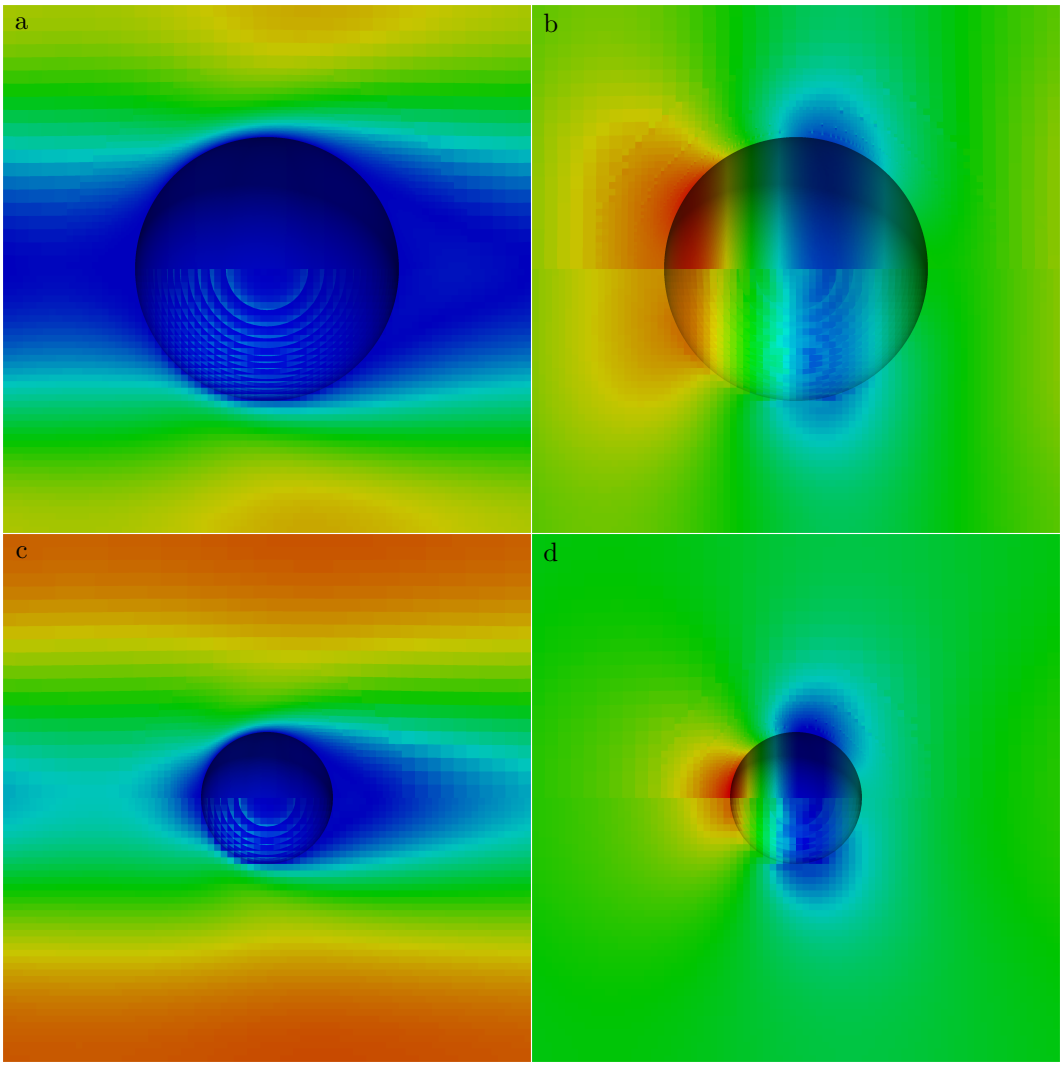

Figure 2: Each image shows a comparison between conformal (top half) and ID case (bottom half) in terms of the (magnitude of the) velocity (a, c) and pressure field (b, d) for $D = 1\,\mathrm{m}$, $\rho = 40$ (a, b) and $D = 0.5\,\mathrm{m}$, $\rho = 20$ (c, d). For the ID cases, the mesh inside the sphere has been removed in post-processing.

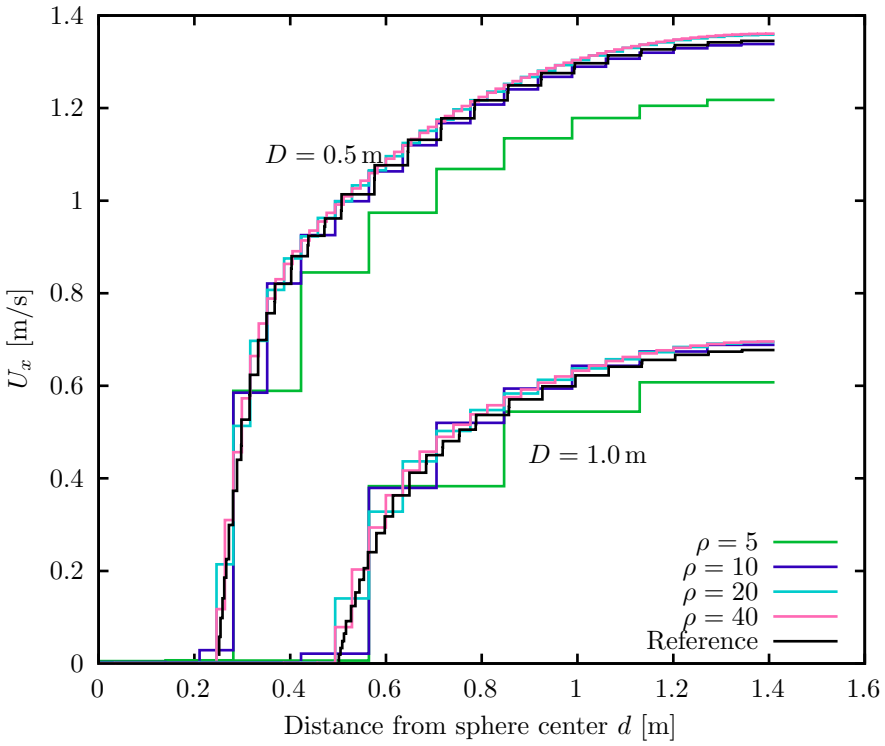

Figure 3: U_x evaluated from the center of the sphere along the direction $(1, 0, 1)$ for four different resolutions using the ID method as well as for the reference conformal mesh case.

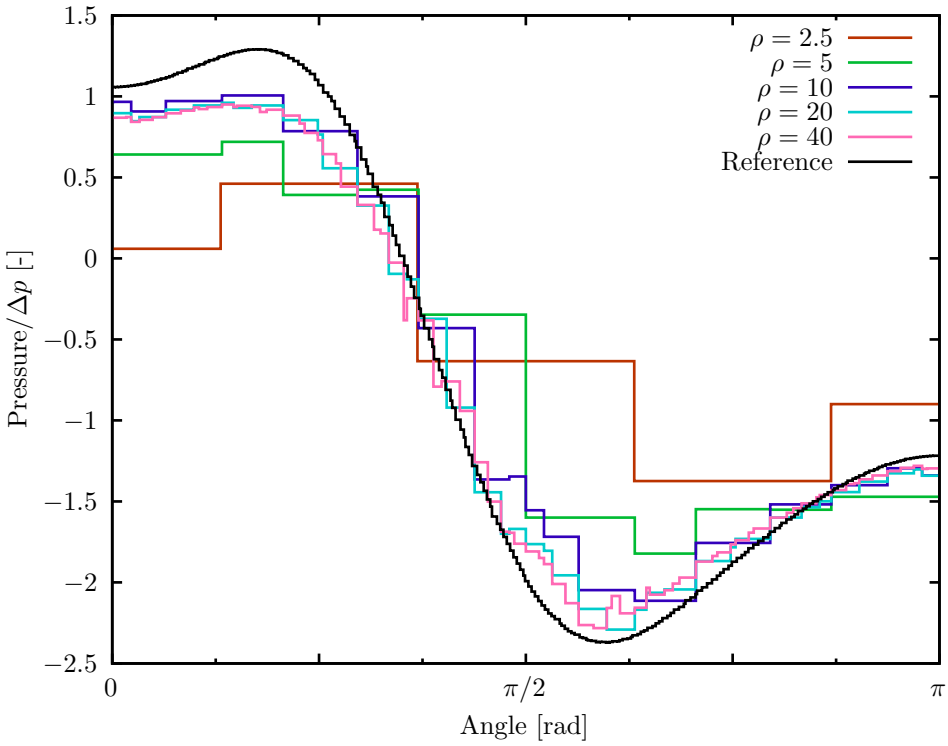

Figure 4: Pressure on the surface of the immersed sphere ($D = 1.0\,\mathrm{m}$) evaluated along a semicircular segment of the equator for five different resolutions using the ID method as well as for the reference conformal mesh case. An angle of 0 corresponds to the upstream direction $(-1, 0, 0)$ and an angle of π to the downstream direction $(1, 0, 0)$.

difference in the pressure result for both methods is also evident when plotting the pressure along the sphere's equator (see Fig. 4). With increasing resolution, the curves again converge towards a limiting curve which, however, does not coincide with the reference conformal mesh curve.

To better quantify the spatial convergence of the flow we evaluate the discrete L^2 norm of the difference between the ID and the conformal solution, which for a field $F \in \{p, U\}$ is given by

$$\mathrm{Err}(F) = \left(\sum_{\text{cells } c} \left(||F_{\mathrm{ID}}(c) - F_{\mathrm{conformal}}(c)||^2 \cdot \mathrm{Volume}_c \right) \right)^{\frac{1}{2}} \tag{6}$$

Because F_{ID} and $F_{\mathrm{conformal}}$ are defined on different meshes we interpolate both

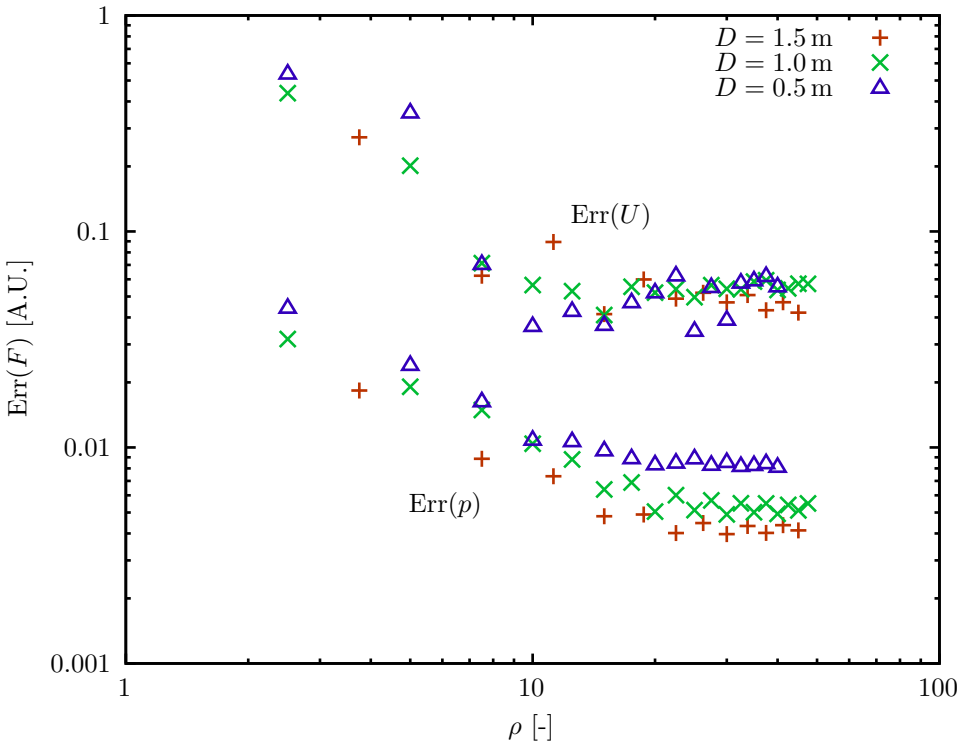

Figure 5: Plots of the discrete L^2 norm of the difference of the pressure field p (bottom) and the velocity field U (top) between the ID and conformal mesh results.

onto a mesh which is at least as fine as any of the two meshes before evaluating $\mathrm{Err}(F)$.

According to the results shown in Fig. 5 for $\mathrm{Err}(p)$ and $\mathrm{Err}(U)$, increasing the resolution above $\rho = 10$ leads to no or negligible improvements in the accuracy of the flow solution in terms of U and p.

3.2. Volume

As discussed in Section 2.1, in the Immersed Domain variant implemented in *cfdemSolverIB*, the force on the sphere is obtained from force-density fields obtained from the flow simulation, which are then summed over all cells that are part of the sphere. Any cell that intersects the sphere is included in the sum, therefore the effective volume used for force calculations V is larger than

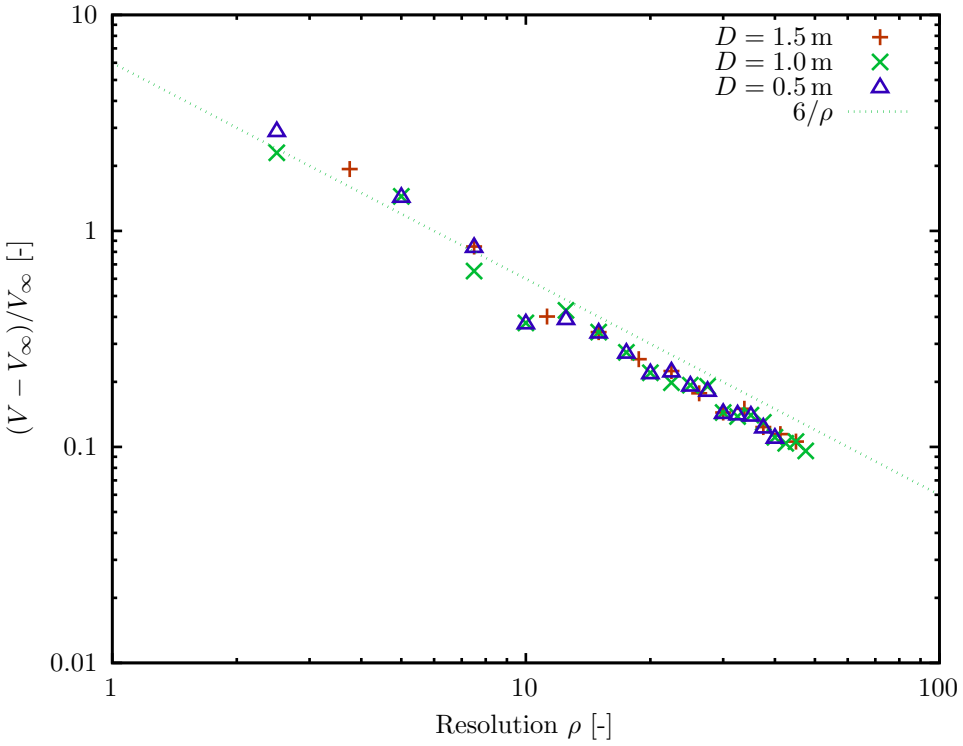

Figure 6: Relative error of the effective volume (symbols) and the expected behaviour according to Eq. (7) (line).

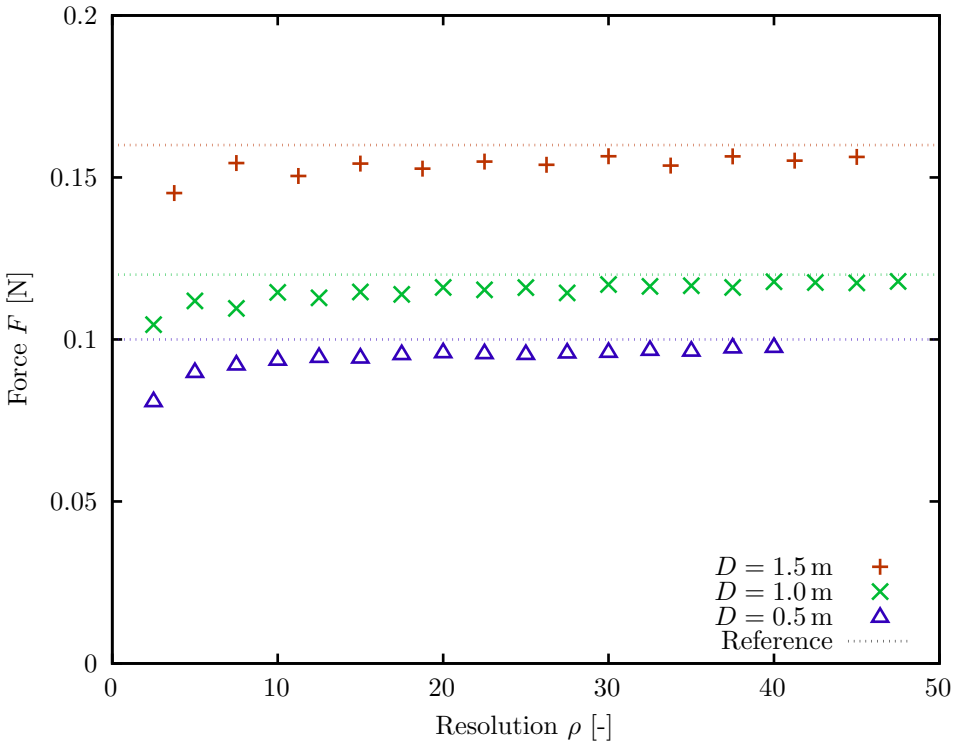

Figure 7: Force F on the sphere obtained from ID simulations as a function of the mesh resolution (symbols) and reference force F_{ref} from Tab. 1 (dashed lines).

the actual sphere volume V_∞ and varies greatly with resolution (Fig. 6).

For a sphere of radius R and cells of linear size c, we expect the error in volume to be related to the volume of a shell of thickness c around a sphere of radius R, so the relative error is expected to be

$$\frac{V - V_\infty}{V_\infty} = \frac{4\pi R^2 c}{4/3\pi R^3} = \frac{3c}{R} = \frac{6c}{D} = \frac{6}{\rho}. \tag{7}$$

We also note in Fig. 6 that convergence is not monotonous which influences the convergence behaviour of the drag force.

3.3. Force

Simulation results for the force F on the sphere are shown in Fig. 7. As the resolution increases, the force approaches a limiting value from below but shows

Diameter [m]	F_{ref}[N]	$F_{\text{conformal}}$[N]	$F_{\text{ID},\rho_{\max}}$[N]
0.5	0.10	0.1007	0.0978
1.0	0.12	0.1200	0.1179
1.5	0.16	0.1600	0.1563

Table 1: Reference forces according to Tab. (5) and numerical results from the conformal and ID simulations for the finest considered resolution.

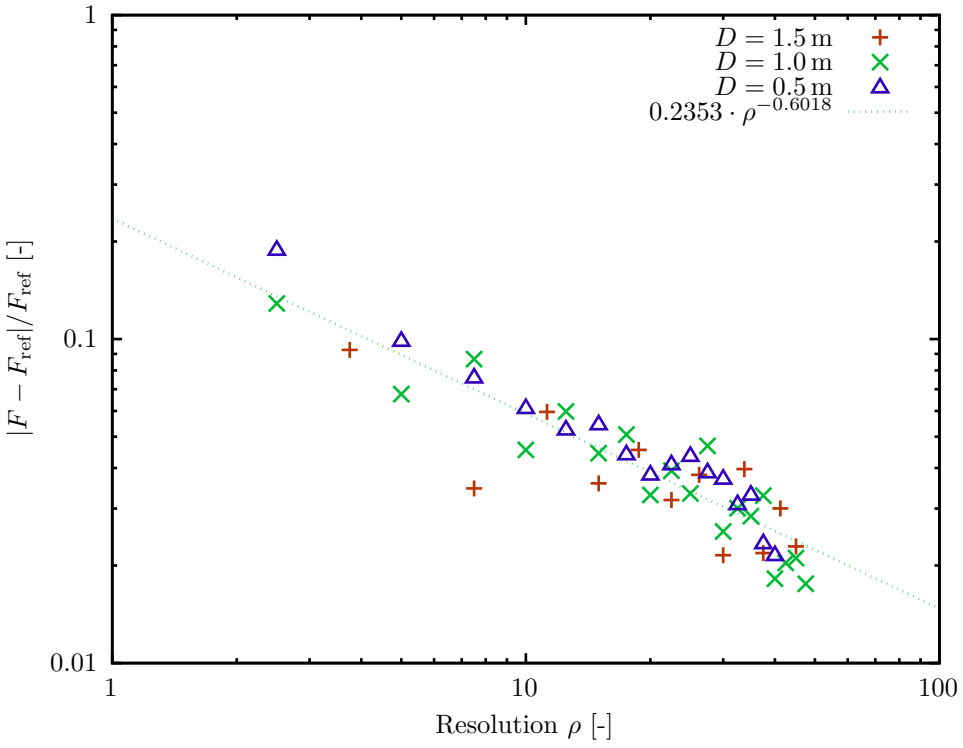

Figure 8: Absolute relative error in F compared to F_{ref} from Tab. 1.

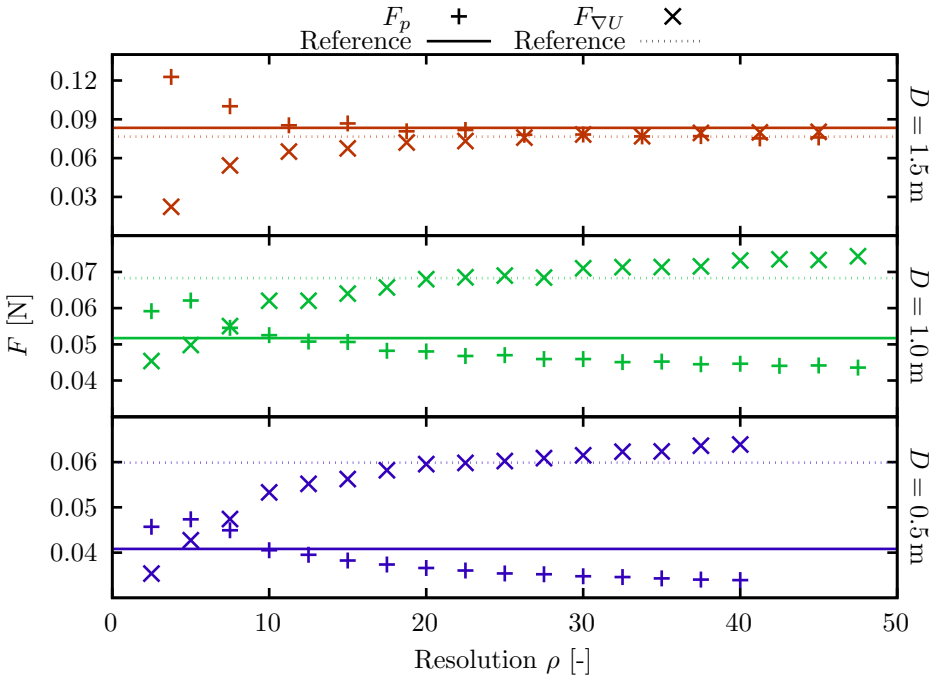

Figure 9: $F_{\nabla U}$ and F_p both change strongly with changing ρ but in opposite directions, keeping F relatively constant.

non-monotonic behaviour. We show the absolute relative error

$$\frac{|F - F_{\mathrm{ref}}|}{F_{\mathrm{ref}}} \tag{8}$$

in Fig. 8. This makes it easier to judge the accuracy of the ID results and also makes the erratic behaviour more apparent.

We note that for the coarsest resolution, F deviates from the reference value by 20 % for $D = 0.5\,\mathrm{m}$ and 9 % for $D = 1.5\,\mathrm{m}$, while for $\rho > 5$, a relative error of less than 10 % is achieved for all studied sphere sizes. Absolute values for F_{ref} and the value obtained from the conformal simulations and the ID simulations on the finest grid $F_{\mathrm{ID},\rho_{\max}}$ are given in Table 1.

3.3.1. Force contributions

Interestingly, while the total force varies by about 10 % over all resolution, the individual contributions F_p and $F_{\nabla U}$ vary as much as 400 % (Fig. 9). However, because their respective trends are in opposite directions, i.e. F_p is over- and $F_{\nabla U}$ undershooting, the changes mostly cancel out, leading to a much smaller change in F.

Moreover, the relative error in each force contribution remains much higher than for the total force, i.e., even for the finest resolution up to 17 % for the contributions compared to 2 % for F.

The reasons behind the convergnce behaviour of the force components is rather complex and not fully understood yet. Assumably, it has its origin in the two-way coupling and the complex interplay between numerics and physics caused by the apparent growth of spheres at low resolution. The best explanation we can offer is an intuition as to why $F_{\nabla U}$ decreases when decreasing the resolution: As the effective sphere volume increases as the resolution gets coarser, the effective channel width decreases, whereas the pressure difference remains constant. This leads to a lower flow velocity (which manifests itself in a smaller Reynolds number) and consequently, a smaller gradient at the surface. Compare also Fig. 10 for the behavior of the Reynolds number with respect to the resolution.

3.3.2. Order of convergence and the "resolution-free" force

In [12], Tang et. al. estimate the "resolution-free" force as the limit of F for infinite ρ, the force obtained from a hypothetical ID simulation carried out at infinite resolution. Their analysis hinges on F having the same order of convergence as their spatial differencing scheme, which in their case is of order two, allowing them to fit their results with a function of the form $F = F_\infty + C\rho^{-2}$.

Despite also using second order accurate schemes for all derivatives, our F does obviously not converge quadratically. Fitting a power law to the absolute relative error in F (Fig. 8) gives a convergence exponent of about 0.6, though

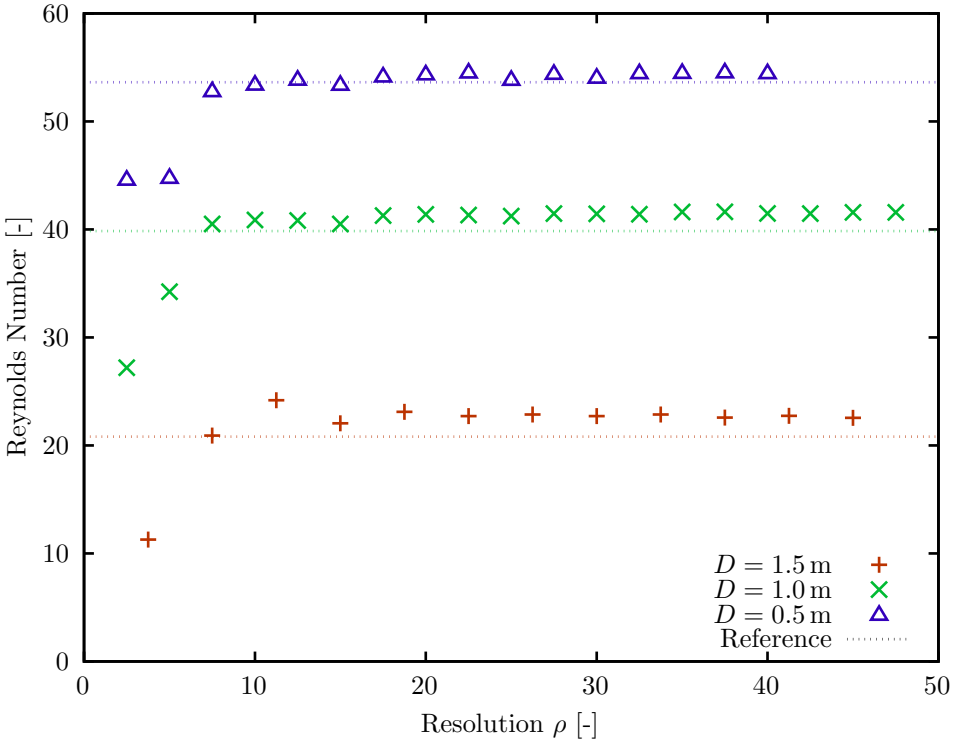

Figure 10: Dependency of superficial Reynolds number on the resolution.

it remains unclear whether F actually converges towards F_{ref}.

Furthermore, because of the limited range of F and the strong fluctuations, we cannot confidently fit our data directly with any power law. The convergence exponent from Fig. 8 cannot be used for this purpose, because any parameters obtained from it are very sensitive to the choice of F_{ref}.

4. Conclusions

We set out to determine whether coarsely resolved ID simulations provide sufficent accuracy to be used in coupled CFD-DEM simulations. Our results indicate that badly resolved simulations (~ 2.5 cells per diameter) provide coupling forces accurate to about $\sim 20\,\%$, while already moderately well resolved flows (~ 10 cells per diameter) are accurate to about $7\,\%$. The accuracy might be improved by using the results from Section 3.3 to correct for systematic volume dependent errors.

While the results give a positive indication that this use of the ID method may indeed be possible, these simulations provide only small clues as to whether it is computationally feasible. Using a transient solver and rather long simulation times to approximate a steady state, we notice simulations times increase drastically with resolution. But as we note in the previous paragraph, force results are quite accurate even for small to moderate resolutions, and in these cases simulation durations were sufferable. Also, in all cases, the force converged rather quickly compared to other quantities like Reynold's number. Therefore, we expect acceptable performance in a dynamic simulation.

Acknowledgement

Part of this work was supported by the IPROCOM Marie Curie initial training network, funded through the People Programme (Marie Curie Actions) of the European Union's Seventh Framework Programme FP7/2007-2013/ under REA grant agreement No. 316555.

References

[1] P. A. Cundall, O. D. L. Strack, A discrete numerical model for granular assemblies, Géotechnique 29 (1) (1979) 47–65. doi:10.1680/geot.1979.29.1.47.

[2] N. Deen, M. V. S. Annaland, M. V. der Hoef, J. Kuipers, Review of discrete particle modeling of fluidized beds, Chemical Engineering Science 62 (1–2) (2007) 28–44. doi:10.1016/j.ces.2006.08.014.

[3] C. Bierwisch, T. Kraft, H. Riedel, M. Moseler, Three-dimensional discrete element models for the granular statics and dynamics of powders in cavity filling, Journal of the Mechanics and Physics of Solids 57 (1) (2009) 10–31. doi:10.1016/j.jmps.2008.10.006.

[4] C. S. Peskin, Flow patterns around heart valves: A numerical method, Journal of Computational Physics 10 (2) (1972) 252–271. doi:10.1016/0021-9991(72)90065-4.

[5] R. Glowinski, T.-W. Pan, T. I. Hesla, D. D. Joseph, J. Périaux, A distributed lagrange multiplier/fictitious domain method for flows around moving rigid bodies: Application to particulate flow, International Journal for Numerical Methods in Fluids 30 (8) (1999) 1043–1066. doi:10.1002/(SICI)1097-0363(19990830)30:8<1043::AID-FLD879>3.0.CO;2-Y.

[6] A. A. Shirgaonkar, M. A. MacIver, N. A. Patankar, A new mathematical formulation and fast algorithm for fully resolved simulation of self-propulsion, J. Comput. Phys. 228 (7) (2009) 2366–2390. doi:10.1016/j.jcp.2008.12.006.

[7] G. Hou, J. Wang, A. Layton, Numerical methods for fluid-structure interaction — a review, Communications in Computational Physics 12 (2) (2012) 337–377. doi:10.4208/cicp.291210.290411s.

[8] S. Haeri, J. Shrimpton, On the application of immersed boundary, fictitious domain and body-conformal mesh methods to many particle multiphase

flows, International Journal of Multiphase Flow 40 (2012) 38–55. doi:10.1016/j.ijmultiphaseflow.2011.12.002.

[9] M.-C. Lai, C. S. Peskin, An immersed boundary method with formal second-order accuracy and reduced numerical viscosity, Journal of Computational Physics 160 (2) (2000) 705–719. doi:10.1006/jcph.2000.6483.

[10] B. E. Griffith, C. S. Peskin, On the order of accuracy of the immersed boundary method: Higher order convergence rates for sufficiently smooth problems, Journal of Computational Physics 208 (1) (2005) 75–105. doi:10.1016/j.jcp.2005.02.011.

[11] Y. Mori, C. S. Peskin, Implicit second-order immersed boundary methods with boundary mass, Computer Methods in Applied Mechanics and Engineering 197 (25–28) (2008) 2049–2067. doi:10.1016/j.cma.2007.05.028.

[12] Y. Tang, S. Kriebitzsch, E. Peters, M. van der Hoef, J. Kuipers, A methodology for highly accurate results of direct numerical simulations: Drag force in dense gassolid flows at intermediate reynolds number, International Journal of Multiphase Flow 62 (2014) 73–86. doi:10.1016/j.ijmultiphaseflow.2014.02.009.

[13] B. Blais, M. Lassaigne, C. Goniva, L. Fradette, F. Bertrand, A semi-implicit immersed boundary method and its application to viscous mixing, Computers & Chemical Engineering 85 (2016) 136–146. doi:10.1016/j.compchemeng.2015.10.019.

[14] T. Ye, R. Mittal, H. Udaykumar, W. Shyy, An accurate cartesian grid method for viscous incompressible flows with complex immersed boundaries, Journal of Computational Physics 156 (2) (1999) 209–240. doi:10.1006/jcph.1999.6356.

[15] M. Meyer, A. Devesa, S. Hickel, X. Hu, N. Adams, A conservative immersed interface method for large-eddy simulation of incompressible flows, Journal

of Computational Physics 229 (18) (2010) 6300–6317. doi:10.1016/j.jcp.2010.04.040.

[16] P. Pepiot, O. Desjardins, Direct numerical simulation of dense particle-laden flows using a conservative immersed boundary technique, in: Proceedings of the CTR Summer Program, 2010.

[17] O. M. Curet, I. K. AlAli, M. A. MacIver, N. A. Patankar, A versatile implicit iterative approach for fully resolved simulation of self-propulsion, Computer Methods in Applied Mechanics and Engineering 199 (37–40) (2010) 2417–2424. doi:10.1016/j.cma.2010.03.026.

[18] A. Hager, C. Kloss, S. Pirker, C. Goniva, Efficient realization of a resolved CFD-DEM method within an open source framework, in: Proc. Open Source CFD International Conference, 2011.

[19] A. Hager, C. Kloss, S. Pirker, C. Goniva, Parallel resolved open source CFD-DEM: Method, validation and application, The Journal of Computational Multiphase Flows 6 (1) (2014) 13–27. doi:10.1260/1757-482X.6.1.13.

[20] R. J. Hill, D. L. Koch, A. J. C. Ladd, Moderate-reynolds-number flows in ordered and random arrays of spheres, Journal of Fluid Mechanics 448 (2001) 243–278. doi:10.1017/S0022112001005936.

[21] R. Beetstra, M. A. van der Hoef, J. A. M. Kuipers, Drag force of intermediate reynolds number flow past mono- and bidisperse arrays of spheres, AIChE Journal 53 (2) (2007) 489–501. doi:10.1002/aic.11065.

[22] E. Fattahi, C. Waluga, I. Wohlmuth, Rüde, Manhart, Helmig, Pore-scale lattice boltzmann simulation of laminar and turbulent flow through a sphere pack, CoRR abs/1508.02960.
URL http://arxiv.org/abs/1508.02960

[23] S. I. Martynov, Viscous flow past a periodic array of spheres, Fluid Dynamics 37 (6) (2002) 889–895. doi:10.1023/A:1022396112523.

[24] C. Goniva, B. Blais, S. Radl, C. Kloss, Open source CFD-DEM modelling for particle-based processes, in: 11th International Conference on Computational Fluid Dynamics in the Minerals and Process Industries, 2015.

[25] H. G. Weller, G. Tabor, H. Jasak, C. Fureby, A tensorial approach to computational continuum mechanics using object-oriented techniques, Comput. Phys. 12 (6) (1998) 620–631. doi:10.1063/1.168744.

[26] C. Kloss, C. Goniva, A. Hager, S. Amberger, S. Pirker, Models, algorithms and validation for opensource DEM and CFD-DEM, Progress in Computational Fluid Dynamics, An Int. J. 12 (2/3) (2012) 140–152. doi:10.1504/PCFD.2012.047457.

[27] R. I. Issa, Solution of the implicitly discretised fluid flow equations by operator-splitting, J. Comput. Phys. 62 (1) (1986) 40–65. doi:10.1016/0021-9991(86)90099-9.

[28] P. M. Adler, Porous Media: Geometry and Transports, Butterworth-Heinemann, 1992.